

UNIAXIAL COMPRESSION PERFORMANCE OF ECC BASED ON NUMERICAL SIMULATION

Jun Zhao¹, Yuxin Xie, Shangxin Zhang², Chunling Yan¹, Hongbo Xiao¹, Songqiang Wan¹, Jingli Yang¹, Chenjie Hao¹, Junhua Guo¹, Xingyao Wang¹, Chongjin Li¹, Han Song¹, Long Liu¹

- 1. Henan Province Engineering Research Center of Material for Reinforcing Concrete Structure & Anyang Engineering Research Center of High ductility Concrete Structure, Anyang Institute of Technology, West section of Yellow River Avenue, Anyang 455000, China; 20160913@ayit.edu.cn*
- 2. Hennan Changming Engineering Consulting Co., Ltd., 626880991@qq.com*

Received: 12.12.2024
Received in revised form: 19.07.2025
Accepted: 23.03.2026

ABSTRACT

In many studies on the compressive properties of engineering cement-based composites (ECC), there are relatively few mesoscopic studies on the dosage and length of PVA fibers. To explore the influence of internal fibers of ECC on its compressive performance, this paper established a two-dimensional distribution model of PVA fibers in the matrix through random placement and generation algorithms. Firstly, an overview of previous experiments was provided. The ECC finite element (FE) model was developed using ABAQUS, and the simulation outcomes were contrasted with the experimental stress-strain curves to validate the model's viability. On this basis, parameter analysis was carried out to study the impact of different PVA fiber content and length in ECC on its compressive characteristics under vertical axial compression, and the characteristic values of the stress-strain curves of ECC with differing PVA fiber content and length under vertical axial compression were analyzed. The findings indicate that the ECC containing 2% PVA fiber with a length of 12 mm exhibits optimal compressive strength, and the yield stress and peak stress can reach 47.25 MPa and 54.96 MPa, respectively. When the fiber content is below 2% and the length ranges from 10 mm to 12 mm, the yield stress and peak stress of ECC progressively rise with increasing fiber content and length. Conversely, when the fiber content exceeds 2% within the same length range, the yield stress and peak stress of ECC exhibit a declining trend as fiber content increases. This research offers a reference for the judicious choice of fiber content and length to enhance the compressive capabilities of ECC.

KEYWORDS

ECC; FE model, PVA fiber, Uniaxial compression, Stress-strain curve

INTRODUCTION

Concrete is now recognised as the most widely utilised man-made material globally due to its superior physical and mechanical characteristics, easy access to materials and low cost.

However, because to its inadequate crack resistance and ductility, reinforced concrete (RC) structures will develop microcracks under large compressive stress, causing serious durability problems [1]. In the 1990s, Victor Li developed a high-ductility concrete called engineered cement composite (ECC) [2,3]. With the help of internal fibers, this material can improve the toughness and ductility of concrete and show good material properties. Among them, PVA fiber possesses approximately 1/8 the strength of high modulus PE fiber, while exhibiting superior tensile strength and elastic modulus compared to polypropylene (PP) fiber [4]. It has excellent mechanical properties [5], durability [6] and crack resistance [7], and has been widely used in various fiber reinforcement technologies. ECC is mainly used in bridge deck paving, RC beams and columns, dam repair and other projects [8]. The application scenario is shown in Figure 1. Its excellent compressive performance can effectively improve the compressive bearing capacity of the structure.

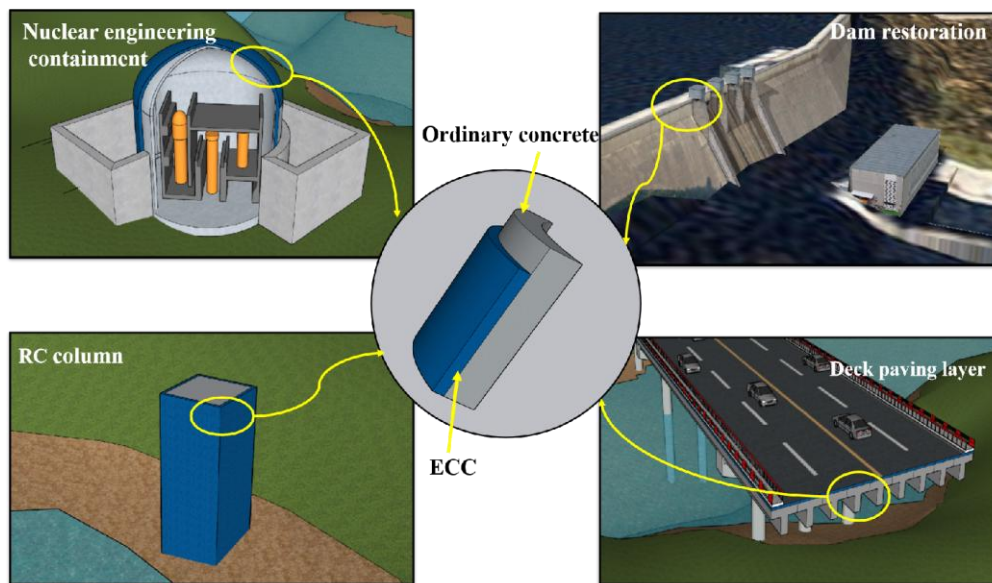


Fig. 1 – Application scenarios of ECC

In previous studies, scholars have conducted extensive research and discussions on the compression performance of ECC. Zhou et al. [9] performed an experimental investigation on the compression properties of ECC and revealed that the compressive strength of ECC is 20 to 80 MPa. Fischer et al. [10] found through uniaxial compression tests that the strength of ECC materials approaches that of high-strength concrete. In addition, the distribution of fibers has affected the ultimate compressive strain of ECC. Hu et al. [11] made uniaxial compression evaluation on ECC. The outcome showed that including fibers can improve the toughness of the matrix, altering its failure mode from brittle to ductile. The axial compressive stress-strain curve of ECC after peak load is gentler than that of ordinary concrete, and the ultimate compressive strain is considerably greater than that of conventional concrete. Singh [12] showed through experimental research that within a certain range, as the fiber length and fiber diameter increase, the flexural strength and final tensile strength of ECC increase accordingly. However, these studies are limited to experiments, which require a lot of time and effort, are costly, and cannot accurately observe the internal compression of ECC. Therefore, it is necessary to adopt a new method to study the compressive performance of ECC.

Finite element (FE) model can be used as an effective method to study the stress condition of materials [13-15]. At present, a large number of scholars have established numerical models from macroscopic and microscopic perspectives to study the compressive performance of ECC. Hung et al. [16] established a three-dimensional FE model of ECC and embedded the constitutive model material subroutine UMAT into LS-DYNA to describe the mechanical behavior of ECC. At

the same time, a three-dimensional FE model of ECC plate and two-span continuous beam was established for numerical calculation. Gencturk et al. [17] applied a macroscopic numerical model that simulated the stress performance of ECC under cyclic load and contrasted it to experimental findings. The simulation results were consistent with the experimental results, proving the correctness of the model. Li et al. [18] used ABAQUS to numerically simulate the ECC frame node under low-cycle reciprocating load. The results showed that the axial compression ratio significantly influenced the compressive performance of the ECC frame node. On the other hand, the microscopic scale can study ECC materials at a deeper level, and many scholars have undertaken research related to the microscopic numerical simulation of concrete and fiber concrete. Ren [19] implemented a random placement algorithm for concrete aggregates through MATLAB and established a microscopic geometric model of fiber concrete, laying the foundation to support the subsequent research of the mechanical properties of concrete through microscopic FE methods. Liang et al. [19] successfully established a three-dimensional microscopic model of steel fiber concrete based on Delaunay triangulation and verified it.

Compared with the microscopic numerical simulation of traditional fiber concrete, the small diameter and large number of PVA fibers in ECC materials will bring certain challenges to the random placement of fibers in the matrix. In addition, the connection between PVA fibers and the matrix is crucial and it is necessary to reflect it in the numerical simulation. However, in many studies on the compressive performance of ECC, there are relatively few mesoscopic studies on the dosage and length of PVA fibers. Therefore, this paper conducts an in-depth study on the compressive properties of ECC with varying PVA fiber content and fiber length. First, ECC is simplified into a two-phase composite material of cement mortar matrix and fiber, and a fiber random generation algorithm is developed using Python software. The FE model constructed with ABAQUS is applied to analyze the mechanical properties of ECC under uniaxial compression, and is likened with existing data from experiments to validate the model's accuracy. Further simulations of different PVA fiber content and length in ECC are performed, and the mechanical properties of ECC under uniaxial compression are evaluated by yield stress, peak stress, EAC and Poisson's ratio.

Experimental Overview

According to the "Standard Test Method for Fiber Concrete", in this test, standard-sized cubic test blocks (100 mm × 100 mm × 100 mm) were used to study the compressive mechanical properties of ECC. The mechanical properties of ECC under compression were studied. The uniaxial compression test was conducted on a universal testing machine (200 t) in accordance with ASTM C469 (ASTM 2002) standard. Transverse and longitudinal strain gauges were affixed to the symmetrical midpoints of the specimen to measure the axial and radial strains. At the same time, two LVDT-50 displacement gauges were symmetrically positioned on the specimen's side to detect axial strain. When loading, the specimen was first loaded continuously and uniformly at an average speed of 1 mm/min to 10 kN. In this process, the specimen was aligned and the effect of the gap between the pressure surface of the specimen and the pad on the test results was eliminated. During the formal loading, the displacement control approach was utilised with an average speed 0.2 mm/min. The specific experimental device can be seen in Figure 2. For detailed material properties and loading information, please refer to reference [20].



Fig. 2 – ECC compression test device

FE model

To examine and evaluate the failure mode of ECC and PVA fibers in ECC under uniaxial compression, a two-dimensional uniaxial compression model of the central section was established using ABAQUS to analyze the compression behavior of ECC. This section gives the two-dimensional modeling method of ECC, the fiber random placement algorithm, and the material constitutive law.

(1) Model establishment

To more realistically reflect the ECC compression test, the FE model size is set to 100 mm × 100 mm. A fixed constraint is set on the bottom surface of the FE model, and a coupling is set between the center point of the top surface and the top surface. A downward displacement load is set at the center point of the top surface, and the load size is 10 mm. In order to make the FE model converge better and be analyzed, the ECC matrix is divided into square grids with a grid size of 2 mm; the fiber is divided into a grid size of 1 mm, as illustrated in Figure 3.

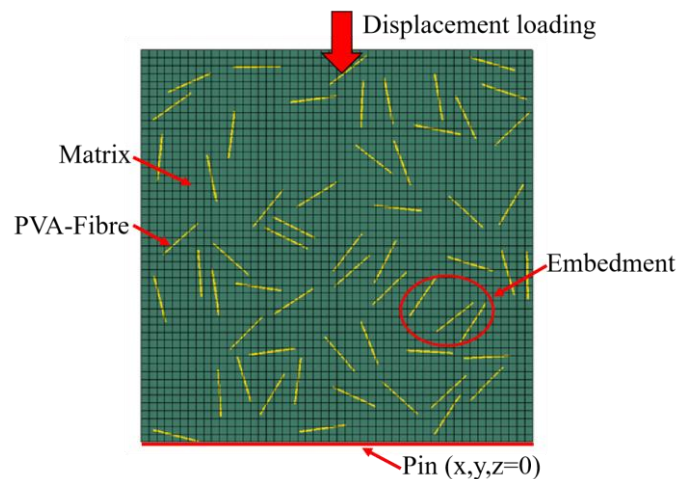


Fig. 3 – Finite element model

(2) Fiber placement algorithm

In order to avoid fiber agglomeration and uneven dispersion and give full play to the role of PVA fibers in ECC materials, PVA fibers should be evenly distributed in the ECC matrix during the ECC casting process. Unlike steel fibers, PVA fibers have a smaller cross-sectional diameter. When establishing a FE model, a large number of fibers in ECC materials often bring certain

difficulties to numerical simulation and model establishment. Therefore, this paper uses the algorithm proposed by Yam [19] to simplify the fibers into straight lines. The calculation formula for the fiber number N is shown in Equation (1):

$$N = \text{round} \left(\frac{4 \times W \times H \times V_f}{100 \times \pi \times d^2 \times L} \right) \quad (1)$$

Where W is the width of the sample, H is the height of the sample, L is the fiber length, d is the fiber diameter, the fiber volume fraction is V_f , and $\text{round}(\cdot)$ is the rounding function.

The fiber random placement geometric model studied by Wu [21], the coordinates (x_i, y_i) of the center point O of the AB fiber are first determined, and the coordinates of the two end points A and B of the fiber are determined according to the fiber length and the fiber inclination angle, as shown in Figure 4.

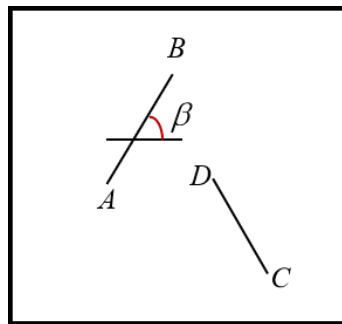


Fig. 4 – Graphic representation of random fiber dispersion

The specific coordinates of the endpoints can be calculated using Equations (2) to (5):

$$x_A = x_i - \frac{l}{2} \times \cos \beta \quad (2)$$

$$y_A = y_i - \frac{l}{2} \times \sin \beta \quad (3)$$

$$x_B = x_i + \frac{l}{2} \times \cos \beta \quad (4)$$

$$y_B = y_i + \frac{l}{2} \times \sin \beta \quad (5)$$

Where l is the fiber length, and β is the angle between the fiber and the horizontal line.

After randomly generating the endpoint coordinates of all fibers, the “Line()” geometric modeling method provided by the ABAQUS secondary development interface is used to connect the two endpoint coordinates of all fibers into a straight line, thereby obtaining a geometric model of random fiber placement.

(3) Material constitutive

In the FE method, the PVA fiber is considered to be a linear elastic material, and the specific values are provided in Table 1. Due to the random distribution characteristics of the fiber, a beam element is used for modeling, and its diameter is 0.1 mm. The fiber and the matrix are connected in an internal manner, that is, all the nodes of the fiber are connected to the ECC matrix.

Tab. 1 - Fiber parameters

Fiber name	Density (g/mm ³)	Tensile strength (MPa)	Modulus of elasticity (MPa)	Fiber diameter (μm)
PVA	1.3	1620	43	12

The concrete plastic damage model may properly explain the damage variation law of materials based on cement. Therefore, this research utilizes the elastic-plastic damage model in the constitutive model of the ECC matrix. For the constitutive model of the matrix, the literature [22,23] demonstrates that the mechanical characteristics of concrete are comparable to those of cement mortar, thus the concrete plastic damage model is employed to simulate the matrix.

The matrix strength in the FE simulation adopts the measured compressive capacity of the cubic specimen, which is 50 MPa, elastic modulus is 31 GPa, Poisson's ratio is 0.2, and density is 2.5 g/mm³. In ABAQUS, several essential values in the plastic damage model need to be specified to specify the yield and failure criteria of the matrix. The particular parameter values are presented in Table 2.

Tab. 2 - Some special values in plastic damage model

Angle of expansion	Eccentricity	f_{b0}/f_c	K	Viscosity coefficient
38	0.1	1.16	0.6666667	1E-5

Results and discussion

The FE model was examined and the outcomes of the simulation were compared with the experimental findings of Xu [20] to verify the reliability of the FE model. Based on the model verification, a detailed parameter study was carried out. By analyzing different PVA fiber dosages and lengths, the stress-strain curves, yield stress, peak stress, EAC and Poisson's ratio of the specimens under different parameters were obtained to explore the mechanical properties of ECC under uniaxial compression.

(1) Stress-strain curve

The full stress-strain curves of ECC obtained by the FE model and the test are shown in Figure 5. It can be seen from the figure that both sets of stress-strain curves show a trend of increasing first and then decreasing. The yield stress and peak stress in the model analysis are 47.25 MPa and 54.96 MPa, respectively, which are 3.5% and 8.2% higher than the yield stress and peak stress obtained in the test. This is because the PVA fibers in the FE model are evenly distributed in the ECC, so that the load can be evenly stressed when bearing the load, resulting in a larger result. In addition, the FE model is simplified into a two-dimensional model to simulate the compression of the central section of the simulated specimen, which is larger than the test result. On the other hand, the peak strain in the FE analysis is 0.00339, which is slightly different from the peak strain of ordinary mortar and is also close to the peak strain of 0.004 in the test. It may also be determined by the study findings of the FE model that ECC can continue to bear a certain load after the peak stress, which is consistent with the results in the test and the law obtained by Li et al. [24].

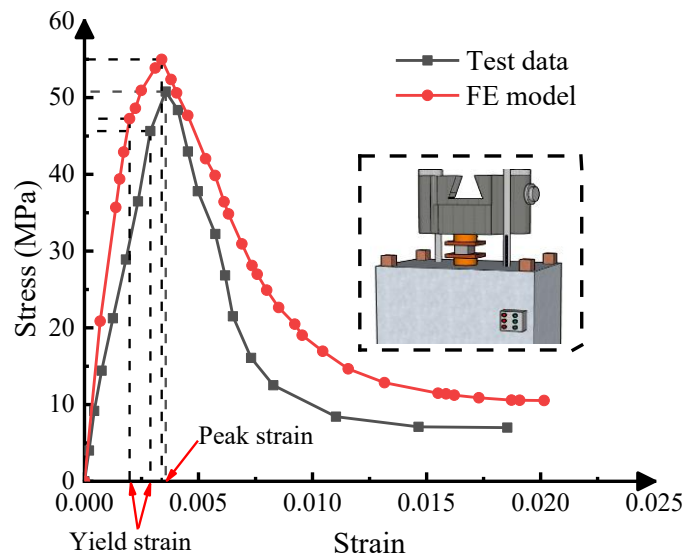


Fig. 5 – FE model analysis results and experimental stress-strain curve

(2) Destruction status

Figure 6 (a), the experimental phenomenon shows that the failed mode of ECC is different from the failure mode of the four-cornered pyramid surface of ordinary concrete. Through the bridging effect of the fiber at the break, the lateral expansion of the middle part of the cube becomes smaller, and the external bulging phenomenon of the fiber concrete in the middle part does not occur. At the same time, the strength of the test sample has been enhanced to a certain level. After reaching the peak load, ordinary concrete breaks rapidly and shows brittle failure. In the final failure stage of the ECC specimen, the hissing sounds of fiber splitting and pulling out can be distinctly heard. The specimen does not show brittle failure, and the specimen has good integrity, reflecting that ECC has good toughness.

Figure 6 (b) shows the compressive damage cloud map of the ECC compressive specimen. It can be seen that when the peak stress is reached, obvious damage occurs in the 45° direction inside the ECC compressive specimen, and the cracks in the middle area of the specimen continue to expand along the 45° direction until they are connected, resulting in X-shaped damage, which is consistent with the experimental results. Due to the existence of fibers between the connected fissures, when the stress continues to rise, the bridging effect of the fibers allows the ECC compressive specimen to continue to withstand larger loads, but at this time the internal damage of the ECC compressive specimen is already quite serious, and the cracks will continue to expand.

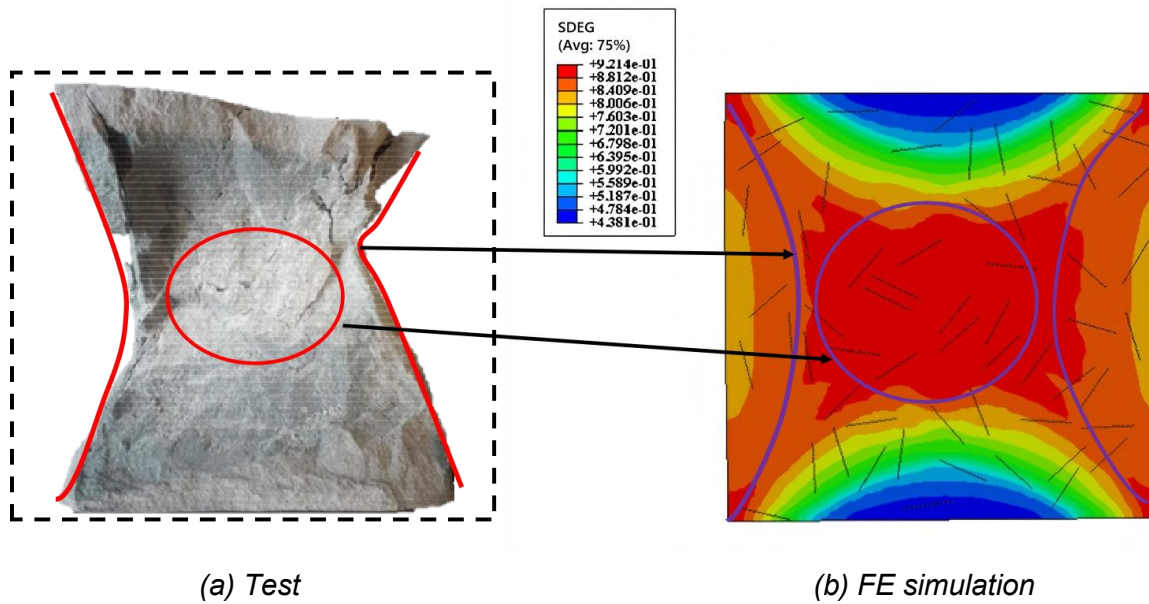


Fig. 6 – Comparison of FE model failure and experimental phenomena

In summary, by comparing the stress-strain curves and failure modes in the FE model and the experiment, it is shown that the FE model can better reflect the mechanical properties of ECC under compression.

Parameter study

Based on the model verification, the FE model was used to conduct parameter research. The mechanical features of ECC under compression were examined by varying the dosage and length of PVA fibers in the ECC mixture. The specific research variables are shown in Table 3.

Tab. 3 - Details of parametric analysis

Serial No.	Fiber ratio(%)	Fiber length(mm)
ECS-1	0.4	12
ECS-2	0.8	12
ECS-3	1.2	12
ECS-4	1.6	12
ECS-5	2	12
ECS-6	2.4	12
ECS-7	2.8	12
ECS-8	3.2	12
ECS-9	3.6	12
ECS-10	2	10
ECS-11	2	11
ECS-12	2	13
ECS-13	2	14

(1) Fiber content

The stress-strain relationship under uniaxial compression contains important mechanical performance indicators, which can fully reflect the deformation characteristics and the whole process of destruction of the material at each stress stage. It is a material physical condition necessary for structure and component design and nonlinear analysis. To investigate the influence of the fiber quantity on the compressive performance of ECC, the fiber content was incrementally raised by 0.4% for the parameter study. The ECC compressive stress-strain curve obtained by FE model analysis is shown in Figure 7.

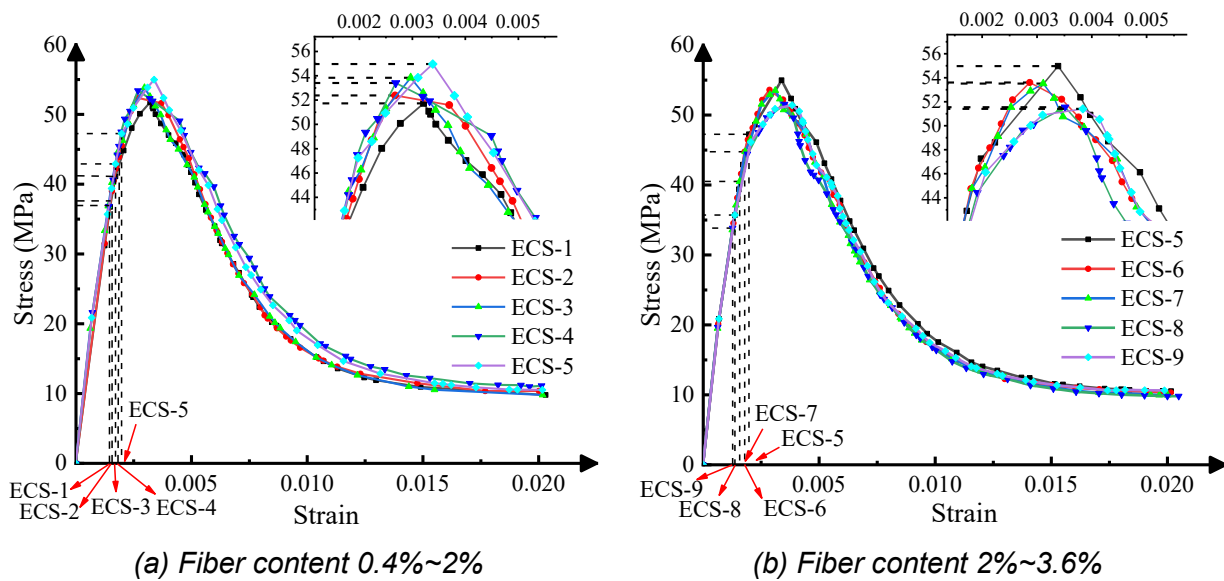


Fig. 7 – Stress-strain curves of different fiber content

As illustrated in Figure 7, the shape of the stress-strain curve of ECC is similar to the compressive curve of ordinary concrete, which is a skewed single-peak curve. In the initial stage, the slope of the stress-strain curve of ECC is close to a straight line. As the load gradually increases, some fibers are broken, and the curve's slope alters markedly upon attaining the yield stress. When the fiber content is 0.4%~2%, as the fiber content increases, the yield strain increases from 0.0013 to 0.002, which is 1.5 times higher. The addition of fiber enhances the compressive capacity of ECC. When the fiber content is 2% to 3.6%, as the fiber content increases, the yield strain decreases from 0.002 to 0.0011, which is a decrease of 45%. After the curve enters the strengthening stage, the peak strains of ECS-1 to ECS-9 are between 0.0025 and 0.0035, and the change is not obvious. Overall, when the fiber length is 2%, the yield stress and peak stress of ECC reach the maximum value, and it has good compressive bearing capacity.

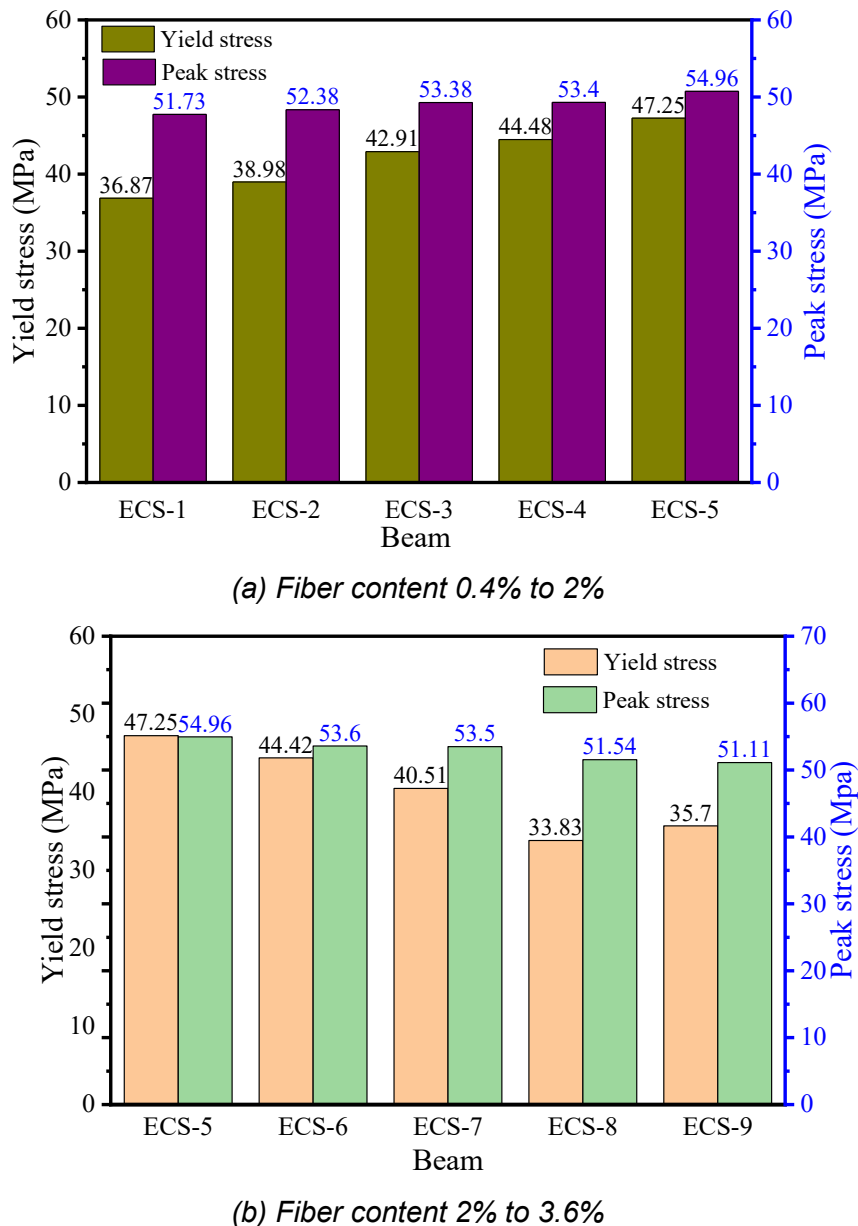


Fig. 8 – Yield and peak stress of different fiber contents

Figure 8 lists the yield stress and peak stress of ECC with different fiber content. As shown in Figure 8 (a), when the fiber content is 0.4% to 2%, the yield stress and peak stress of ECC gradually increase with the increase of fiber content. Compared with ECS-1, the yield stress and peak stress of ECS-5 are 47.25 MPa and 54.96 MPa, respectively, which are increased by 28.1% and 6.2%, respectively. This can be explained that the addition of fiber can enhance the ductility and toughness of ECC, improve the compressive strength of the material, and enable ECC to withstand greater stress. As illustrated in Figure 8 (b), when the fiber content is 2% to 3.6%, the yield stress and peak stress of ECC progressively diminish as fiber content increases. Compared with ECS-5, the yield stress of ECS-8 is 33.83 MPa, which is a decrease of 28.4%. Compared with ECS-5, the peak stress of ECS-9 decreases from 54.96 MPa to 51.11 MPa, which is a decrease of 7.0%. This result occurs because too many fibers are unevenly distributed inside the concrete, which causes the surrounding fibers to gather together, resulting in fiber bundling, which causes

the ECC's compressive performance to decrease. Nonetheless, owing to the bridging action of the fibers, the ECC can persist in withstanding the pressure.

Tab. 4 - EAC and Poisson's ratio of different fiber content

Test block	ECS-1	ECS-2	ECS-3	ECS-4	ECS-5	ECS-6	ECS-7	ECS-8	ECS-9
EAC (J/m^2)	0.439	0.446	0.449	0.485	0.476	0.459	0.452	0.447	0.456
Poisson's ratio	2.63	2.71	2.89	2.96	2.98	3.00	2.93	2.91	2.90

The energy absorption capacity (EAC) of a material refers to the amount of energy it can absorb when subjected to external force or energy impact [25]. Table 4 illustrates that the EAC progressively rises from ECS-1 to ECS-4 as fiber concentration increases. The energy absorption of ECS-4 is $0.485 J/m^2$, which is 10.5% higher than that of ECS-1. As the fiber content increases further, the energy absorption shows a decreasing trend. Compared with ECS-4, the energy absorption values of ECS-5 and ECS-8 are $0.476 J/m^2$ and $0.447 J/m^2$, respectively, which are 1.8% and 8.5% lower. The energy absorption of ECS-9 is $0.456 J/m^2$, which is 2% higher than that of ECS-8, but the increase is small.

Table 4 gives the Poisson's ratio values of ECC with different fiber content. With an increase in fiber content, the Poisson's ratio initially rises and subsequently declines. Compared with ECS-1, the Poisson's ratio of ECS-6 is 3, an increase of 14.1%. Compared with ECS-6, the Poisson's ratio of ECS-9 is 2.9, a decrease of 3.3%. Simultaneously, it is evident that when fiber content increases, the magnitude of the Poisson's ratio tends to stabilize. The content of PVA fiber influences its interaction with the ECC matrix and the mechanical characteristics of ECC, resulting in a variation of the Poisson's ratio. In fiber-reinforced concrete, the fiber will support a portion of the load when the specimen is subjected to stress. The low elastic modulus of the fiber results in minimal impact on the Poisson's ratio of ECC from the surplus fiber.

(2) Fiber content

In order to study the impact of fiber length on the compressive performance of ECC, the fiber length was gradually increased with 1 mm as the benchmark for parameter study, and the compressive behavior of ECC was analyzed through 5 sets of simulation results. When ECC is subjected to force, relative slippage between fibers will occur, resulting in the fiber being broken. Under uniaxial compression, the strain of ECC changes with the increase of PVA length, as illustrated in Figure 9. As the fiber grows in length, the yield strain and peak strain of ECC initially rise and thereafter decline. Among them, the yield strain and peak strain of ECS-5 reach the maximum, which are 0.002 and 0.0034 respectively.

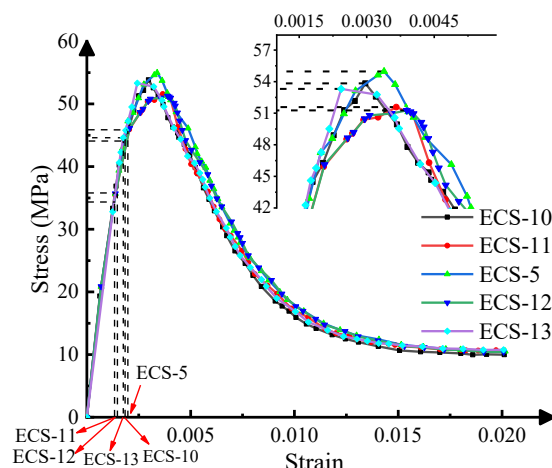


Fig. 9 – Stress-strain curves of different fiber lengths

Figure 10 (a) lists the yield stress values of different fiber lengths. Compared with ECS-10, the yield stress of ECS-11 is 32.81 MPa, which is 26.2% lower. Compared with ECS-11, the yield stress of ECS-5 reaches a maximum value of 47.25 MPa, which is 44.1% higher. The yield strength of ECS-12 is 32.81 MPa, which is 30.5% lower than that of ECS-5 and the same as the yield stress of ECS-11. The yield strength of ECS-13 is 44.60 MPa, which is 35.9% higher than that of ECS-12. The reason for the above pattern is that longer fibers sometimes produce problems such as agglomeration and entanglement in ECC, which in turn affects the uniformity and consistency of the ECC compressive properties, resulting in a decline in the ECC compressive performances.

The peak stress values of different fiber lengths are shown in Figure 10 (b). As the fiber length increases, the peak stress of ECS-5 reaches a maximum value of 54.96 MPa. Compared to ECS-5, the peak stresses of ECS-11 and ECS-12 are 51.57 MPa and 51.26 MPa, respectively, reduced by 6.5% and 7.2%. The peak stresses of ECS-10 and ECS-13 were 53.82 MPa and 53.30 MPa, respectively, which were reduced by 2.1% and 3.1%. The statistics indicate that a fiber length of 12 mm yields optimal compressive performance for ECC.

Tab. 5 - EAC and Poisson's ratio of different fiber content

Test block	ECS-10	ECS-11	ECS-5	ECS-12	ECS-13
EAC (J/m ²)	0.446	0.454	0.476	0.467	0.457
Poisson's ratio	2.92	3.07	2.98	2.89	2.94

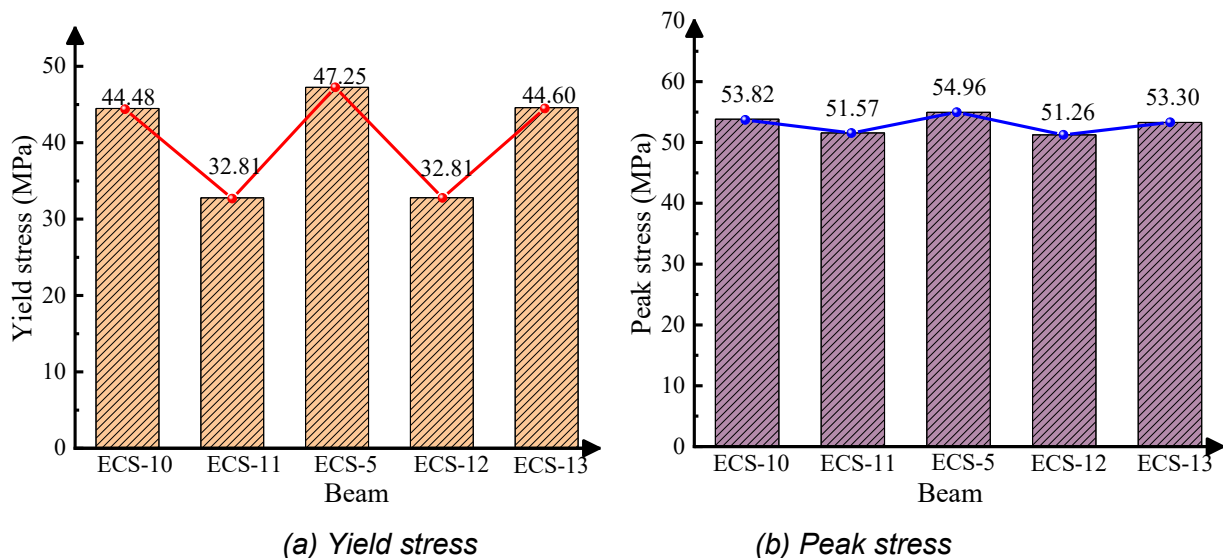


Fig. 10 – Yield and peak stress values at different fiber lengths

Table 5 illustrates that with an increase in fiber length, both the EAC and Poisson's ratio initially rise and thereafter decline. The energy absorption values of ECS-10 and ECS-11 are 0.446 J/m² and 0.454 J/m², respectively, with a small difference. Compared with ECS-10, the energy absorption of EB-5 reaches a maximum value of 0.476 J/m², an increase of about 6.7%. As the fiber length increases further, the energy absorption shows a decreasing trend. Compared with ECS-5, the energy absorption values of ECS-12 and ECS-13 are 0.467 J/m² and 0.457 J/m², respectively, a decrease of about 1.8% and 3.6%. This shows that the EAC of ECS-5 is significantly improved compared with other test groups.

Compared with ECS-10, the Poisson's ratio of ECS-11 is 3.07, an increase of 5.13%. Compared with ECS-11, the Poisson's ratio of EB-12 is 2.89, a decrease of 5.8%. Simultaneously, it is evident that when the fiber length ranges from 10 mm to 14 mm, the augmentation of fiber

length little influences the Poisson's ratio of ECC and has a negligible impact on the overall stiffness of ECC.

CONCLUSIONS

This research studies the impact of PVA fiber content and fiber length on the compressive performance of ECC by numerical simulation method. The numerical model was first validated against experimental data to ensure its accuracy and practical applicability, and the following conclusions are drawn:

- (1) The FE methods can be employed to model the uniaxial compression test of ECC. The derived stress-strain curve and damage occurrence closely align with the experimental findings.
- (2) The stress-strain curve of ECC resembles the complete compressive strength curve of conventional concrete, characterized by a skewed single-peak shape.
- (3) The optimal compressive performance of ECC occurs with a PVA fiber content of 2% and a fiber length of 12 mm. Within the PVA fiber content range of 0.4% to 2%, an increase in fiber content enhances the compressive performance of ECC. The yield stress and peak stress of ECS-5 attain maximum values of 47.25 MPa and 54.96 MPa, respectively. As fiber level exceeds 2%, the compressive performance of ECC diminishes with increasing fiber content.
- (4) Augmenting the fiber length can significantly enhance the compressive characteristics of ECC. The yield stress and peak stress attain their greatest values with a fiber length of 12 mm. When the fiber length is greater than 12 mm, the yield stress, peak stress, and EAC will decrease as the fiber length increases.
- (5) In future research, the authors will further precisely determine the dosage and length of PVA fibers to provide the optimal mechanical properties and offer reliable reference for engineering applications and designs.

ACKNOWLEDGEMENTS

This study is supported by 5 key funds: (1) Science and Technology Planning Project of Anyang, Henan Province, China (2025C01SF168), (2) Start-up Funding of Postdoctoral Innovation Practice Base in Anyang Institute of Technology, Henan Province, China (BHJ2025001), (3) Start-up Funding of Doctoral Research in Anyang Institute of Technology, Henan Province, China (BSJ2025010), (4) Training Program for Young Backbone Teachers in Higher Education Institutions of Anyang Institute of Technology, Henan Province, China (2025004), and (5) Annual Project of the College Students' Innovation and Entrepreneurship Training Program in Henan Province, China (202511330016).

REFERENCES

- [1] Xu T, Zhou Z, Wang M, et al. Damage mechanism of pier concrete subjected to combined compressive stress, freeze-thaw, and salt attacks in saline soil. *Construction and Building Materials*, 2022, 324: 126567. 10.1016/j.conbuildmat.2022.126567.
- [2] Ji J, Zhang Z, Lin M, Li L, Jiang L, Ding Y, et al. Structural application of engineered cementitious composites (ECC): A state-of-the-art review. *Construction and Building Materials* 2023;406:133289. 10.1016/j.conbuildmat.2023.133289.
- [3] Hu Z, Elchalakani M, Yehia S, Ran H, Sadakkathulla MA, Guo X. Engineered cementitious composite (ECC) strengthening of reinforced concrete structures: A state-of-the-art review. *Journal of Building Engineering* 2024;86:108941. 10.1016/j.jobbe.2024.108941.

- [4] Wang LH, Shi WH, Qian LP, Bai YL, Liu SZ, Yang ZQ. Flexural behaviors of GFRP-reinforced Engineered Cementitious Composite (ECC)-concrete composite beams. *Engineering Structures* 2025;332:120097. 10.1016/j.engstruct.2025.120097.
- [5] Shoji D, He Z, Zhang D, et al. The greening of engineered cementitious composites (ECC): A review. *Construction and Building Materials*, 2022, 327: 126701. 10.1016/j.conbuildmat.2022.126701.
- [6] Guan X, Li Y, Liu T, et al. An economical ultra-high ductile engineered cementitious composite with large amount of coarse river sand. *Construction and Building Materials*, 2019, 201: 461-472. 10.1016/j.conbuildmat.2018.12.207.
- [7] Li Y, Li J, Yang E H, et al. Mechanism study of crack propagation in river sand Engineered Cementitious Composites (ECC). *Cement and Concrete Composites*, 2022, 128: 104434. 10.1016/j.cemconcomp.2022.104434.
- [8] Liu D. Development and application of high ductility fiber reinforced cement-based composites. *Transport Business China*, 2022(27): 146-148.
- [9] Zhou J, Pan J, Leung C K Y. Mechanical Behavior of Fiber-Reinforced Engineered Cementitious Composites in Uniaxial Compression. *Journal of Materials in Civil Engineering*, 2015, 27(1): 04014111. 10.1061/(ASCE)MT.1943-5533.0001034.
- [10] Fischer, G., and Li, V. C. (2002). "Effect of matrix ductility on deformation behavior of steel-reinforced ECC flexural members under reversed cyclic loading conditions." *ACI Struct. J.*, 99(6), 781–790.
- [11] Chunhong H, Yane G, Wancong D. Experimental research on compressive performance of ultra high toughness cementitious composites. *Journal of Building Structures*, 2013, 34(12):128-132+154.
- [12] Singh M, Saini B, Chalak H D. Performance and composition analysis of engineered cementitious composite (ECC) – A review. *Journal of Building Engineering*, 2019, 26: 100851. 10.1016/j.jobbe.2019.100851.
- [13] Narimanifar K, Mousavi Ghasemi S A. Evaluating and comparing the bending performance of RC beams fabricated with lightweight aggregate concrete and normal concrete of equivalent strength. *Buildings*, 2024, 15(1): 45. 10.3390/buildings15010045.
- [14] Ellithy M, Hassan A, El-Shafiey T F. Flexural strengthening of RC beams using PGFRP bars embedded in strain-hardening cementitious composites (SHCC). *Engineering Structures*, 2024, 317: 118628. 10.1016/j.engstruct.2024.118628.
- [15] Subramanian N, Solaiyan E, Sendrayaperumal A, et al. Flexural behaviour of geopolymer concrete beams reinforced with BFRP and GFRP polymer composites. *Advances in Structural Engineering*, 2022, 25(5): 954-965. 10.1177/13694332211054229.
- [16] Hung C C, Li S H. Three-dimensional model for analysis of high performance fiber reinforced cement-based composites. *Composites Part B: Engineering*, 2013, 45(1): 1441-1447. 10.1016/j.compositesb.2012.08.004.
- [17] Gencturk B, Elnashai A S. Numerical modeling and analysis of ECC structures. *Materials and Structures*, 2013, 46(4): 663-682. 10.1617/s11527-012-9924-0.
- [18] Li X Q, Ding J, Zhang T, et al. Influence of axial compression ratio on seismic performance of ECC frame nodes of different types. *Journal of Vibration Engineering*, 2022, 35(4): 793-805. 10.16385/j.cnki.issn.1004-4523.2022.04.002.
- [19] Zhigang Ren, Bin Xu, Shuhuai Cheng. A two-dimensional stochastic modeling method for hybrid fiber concrete. *Journal of Wuhan University of Technology*, 2015, 37(4): 53-58.
- [20] Xu Shi-shin, Cai Xiangrong, Zhang Ying-hua. Determination and analysis of full stress-strain curve test of ultra-high toughness cement-based composites under uniaxial compression. *China Civil Engineering Journal*, 2009, 42(11): 79-85. 10.15951/j.tmgcxb.2009.11.009.
- [21] Wu Shaofeng. Study on basic mechanical properties of PVA-ECC materials based on microscopic finite element. *Journal of Water Resources and Architectural Engineering*, 2022, 20(6): 175-181. 10.3969/j.issn.1672-1144.2022.06.026.
- [22] Grote D L, Park S W, Zhou M. Dynamic behavior of concrete at high strain rates and pressures: I. experimental characterization. *International Journal of Impact Engineering*, 2001, 25(9): 869-886. 10.1016/S0734-743X(01)00020-3.
- [23] Li V C. From micromechanics to structural engineering—the design of cementitious composites for civil engineering applications. *Structural Engineering / Earthquake Engineering*, 1994, 10(2): 1-34. 10.2208/jscej.1993.471_1.
- [24] Li Yan, Wen Congge. Study on uniaxial tensile properties of engineering fiber-reinforced cement-based composites PVA-ECC. *Concrete*, 2015(9): 31-35. 10.3969/j.issn.1002-3550.2015.09.009.

- [25] Gopalaratnam V S, Gettu R. On the characterization of flexural toughness in fiber reinforced concretes. *Cement and Concrete Composites*, 1995, 17(3): 239-254. 10.1016/0958-9465(95)99506-O.